IFSCC 2025 full paper (IFSCC2025-270)

NEW GENERATION CERAMIC NANOCOMPOSITES FOR UV FILTERS IN SAFE AND EFFECTIVE SUNSCREENS

Nuwangi P Cooray[1], Philip J Barker[2], Michael Lerch[3], Jung Ho Kim[1], Konstantin Konstantinov[1*]

[1] Institute for Superconducting and Electronic Materials, Faculty of Engineering and Information Sciences, University of Wollongong Innovation Campus, Squires Way, North Wollongong, NSW 2500, Australia

[2] School of Chemistry and Molecular Bioscience, Faculty of Science, Medicine and Health, University of Wollongong, Wollongong, NSW 2522, Australia

[3] Centre for Medical Radiation Physics, School of Physics, Faculty of Engineering and Information Sciences, University of Wollongong, Wollongong, NSW 2522, Australia

* konstan@uow.edu.au

1. Introduction

Inorganic nanoparticulate TiO_2 has been widely used in sunscreen formulations due to its efficient UV absorbance properties resulting from its semiconductor bandgap. At nanoparticulate size, TiO_2 is reported to absorb more than 95% of the incident UV radiation[1]. Yet, this excellent UV filter exhibits an undesired property for the cosmetics industry. The photocatalytic activity (PCA) of TiO_2 is unfavorable for sunscreen applications because the generation of reactive oxygen species (ROS) can not only have biological consequences, such as damage to skin cells and DNA[2], [3], [4], but also hinder the performance of the sunscreen by degrading other organic molecules in the formulation[5], [6]. To overcome these issues, considerable work has been conducted to reduce the photocatalytic activity of these inorganic nano-UV filters without compromising their UV absorbance performance by manipulating crystal phase, particle size, and surface features[7], [8].

Two major crystal phases of TiO_2 that have been employed in UV filter applications are rutile and anatase. Anatase shows higher photocatalytic activity than rutile. However, a mixture of the two phases has often shown comparatively better performance in UV absorbance and photocatalysis applications. On the other hand, in Europe, the SCCS have developed guidelines for safely utilising titanium dioxide nanoparticles in sunscreens. To comply with the guidelines, formulations must not contain anatase and exhibit no photocatalytic properties[9]. Sunscreen manufacturers are constrained by the limited selection of options, as only a handful of commercial rutile nanoaparticles satisfy these criteria. Commercially available rutile nanoparticles are produced by either doping the crystal structure or applying a continuous insulating coating on the surface. Previously, work has shown to apply inert coatings, such as SiO_2 and Al_2O_3[10], [11]. TiO_2 surface decoration with other ROS scavenging materials such as CeO_2, $(BiO)_2CO_3$ and Y_2O_3 has also been studied to maintain UV filtering abilities while suppressing photocatalytic activity[7], [12], [13]. However, a complete surface coating can reduce the UV absorption performance of TiO_2[14] and also result in larger particle size and agglomeration, leading to a non-aesthetic appearance in the formulation.

Due to the above issues, developing methods and materials to suppress the photocatalytic ability of commercial TiO_2 (rutile) while maintaining UV filtering abilities is essential. The deposition of quantum dots (QDs) on the active surface sites of TiO_2 nanoparticles is advantageous, as it has a minimal impact on the overall absorption efficiency. On the other hand, due to the smaller size of the secondary material, composites cause no significant change to the size of the particles. Cerium compounds have been previously studied due to their biocompatibility and UV filtering properties[15]. It has also been shown to display ROS scavenging properties due to its ability to cycle between the Ce^{3+}/Ce^{4+} oxidation states via redox-mediated processes[16]. Although composites of CeO_2 with TiO_2 have been previously investigated for UV filtering applications[8], [12], the surface treatment of commercial rutile nanoparticles with CeO_2 quantum dots (QDs) for sunscreen applications has not been assessed. This study presents commercial rutile nanoparticles surface treatment with CeO_2 QDs to minimise ROS production of TiO_2 upon exposure to UV radiation without compromising its UV absorption properties.

2. Materials and Methods

The materials, chemicals and reagents used throughout this research include Rutile TiO_2 US Research Nanomaterials, Inc, Acerium (III) nitrate hexahydrate ($Ce(NO_3)_3.6H_2O$, 99%, Sigma Aldrich), Ammonium hydroxide (NH_4OH, Sigma Aldrich, 28-30% NH_3 basis), hydrogen peroxide (H_2O_2, 30 wt% in H_2O, Sigma Aldrich), absolute ethanol (CH_3CH_2OH, 96%, ChemSupply) and crystal violet (tris(4-(dimethyl amino) phenyl) methylium chloride, Sigma Aldrich, > 90%).

The synthesis of the CeO_2 encrusted TiO_2 nanoparticles follows a similar process previously outlined by Cardillo et al, (2016)[17]. First, 500 mg of TiO_2 NPs were suspended in 50 mL deionised (DI) water. The suspension was magnetically stirred for 25-30 minutes. $Ce(NO_3)_3.6H_2O$ was added to the suspension according to the Ce/Ti weight ratio of 5 and 10%. The suspension was magnetically stirred while heating at 60±1 °C. Then, 1 mL of concentrated NH_4OH was added dropwise to the mixture, followed by the addition of 1 mL of hydrogen peroxide while stirring. The precipitants were collected via centrifugation (11,000 × g for 10 min) and washed with DI water and ethanol. The resultant material was oven-dried at 100 °C overnight. Finally, the composite powder was obtained by grinding using a mortar and pestle. A sample of pure CeO_2 was prepared in a similar manner without TiO_2 nanoparticles.

The crystal phases of the TiO_2 and the synthesised materials were characterised with PANalytical Aeris XRD using CuKα (λ=1.54059 Å) radiation source.

The nanoparticles' crystal structure and size were studied using a JEOL ARM-200F for Scanning Transmission Electron Microscopy (STEM) and Energy Dispersive Spectroscopy analysis (EDS).

Fluorescence spectra of the UV filter materials were obtained using a Horiba Fluorolog FL3-221 to understand the energy dissipation pathways of TiO_2 and composite samples, with an excitation wavelength of 340 nm.

The UV absorbance of the samples was measured over the range of 800 to 200 nm using a Shimadzu UV-3600 spectrometer from Shimadzu Corporation (Kyoto, Japan) fitted with an integrating sphere. The nanoparticle suspensions were prepared in ethanol at 25 ppm concentration. The bandgap was determined using equation (1):

$$(\alpha h\nu)^n = A(h\nu - E_g) \quad (1)$$

Where, α is the absorption coefficient, h- Planck constant, ν- light frequency, A - a constant, and E_g the band gap. The value of n depends on the type of optical transition of a semiconductor (i.e., n = 2 for a direct transition and n = 0.5 for an indirect transition). The band gap can be estimated from a plot of $(\alpha h\nu)^n$ vs. the energy ($h\nu$).

The photocatalytic activity of the materials was evaluated by observing Crystal Violet (CV) dye degradation by the generation of Reactive Oxygen Species (ROS) from nanoparticles upon exposure to Ultraviolet (UV) radiation in an RPR-200 photochemical reactor (Rayonet, Branford, CT, USA) fitted with 300 nm and 350 nm Hg lamps. A solution of 5 ppm CV was stirred with 5 ppm nanocomposite sample under test and exposed to UV for over 1 hour, with an

aliquot removed every 10 minutes. The degradation of the dye was evaluated by measuring the intensity of the CV absorption maximum at 590 nm, which correlates to the remaining dye concentration. The apparent rate constant k was calculated according to equation (2):

$C_t = C_0 e^{-kt}$ (2)

Where C_t is the concentration of the dye at time t and C_0 is the initial dye concentration.

The prepared nanocomposites were incorporated into a sunscreen formulation comprising the ingredients listed in Table 1.

Table 1 Ingredients List of Sunscreen Formulation

Phase	Chemical name	w/W%		
		HS1	HS2	HS3
A	TiO_2	5.0	0.0	0.0
	10%w $^{QD}CeO_2@TiO_2$	0.0	5.0	0.0
	5%w $^{QD}CeO_2@TiO_2$	0.0	0.0	5.0
	Cetearyl Alcohol (and) PEG-20 Stearate	10.0	10.0	10.0
	Cetyl Stearyl alcohol	5.0	5.0	5.0
	Cocos Nucifera (Coconut) Oil	5.0	5.0	5.0
	Xanthan gum	0.2	0.2	0.2
B	Deionised Water	74.7	74.7	74.7
	Potassium sorbate	0.1	0.1	0.1

*HS: Homemade Sunscreen

In a typical formulation, the commercial Phase A was heated at 80-85°C and mixed using the Toption Intelligent ultrasonic processor for 15-20 minutes. Phase B was separately mixed for 15-20 minutes while heating at 80-85 °C. Then, Phase B was slowly added to Phase A while mixing and further ultrasonicated for 5 minutes. After cooling down to room temperature, sunscreen was obtained. Prepared sunscreen formulations were stored in airtight containers.

The in vitro SPF of sunscreens was assessed using the Diffey equation, following the in-house method as described. In a typical experiment, a sunscreen film with an application rate of 1.3 $mg.cm^{-2}$ was prepared on a quartz substrate. After drying for 15-20 minutes, a Shimadzu UV-3600 spectrometer measured the transmittance through the sunscreen film in the range of 290-400 nm. The obtained data were used to calculate the non-irradiated in vitro SPF using the Diffey equation according to ISO/FDIS 24443:2011[18]. The system was calibrated with reference standard P2.

$$SPF_{in\text{-}vitro} = \frac{\int_{\lambda=290nm}^{\lambda=400nm} E(\lambda)*I(\lambda)*d\lambda}{\int_{\lambda=290nm}^{\lambda=400nm} E(\lambda)*I(\lambda)*10^{-A(\lambda)}d\lambda} \quad \text{------- (3)}$$

Where, E(λ) = Erythema action spectrum (CIE-1987)

I(λ) = Spectral irradiance received from the UV source (SSR for SPF testing)

A(λ) = Absorbance of the sunscreen film

dλ = Wavelength step (1 nm)

3. Results and Discussion

3.1. Crystal Phase, Structural and Elemental Surface Composition

The XRD patterns of the commercial TiO_2, 5%wt$^{QD}CeO_2$@TiO_2 and 10%wt$^{QD}CeO_2$@TiO_2 composites are presented in Figure 1. According to Figure 1 (a) all patterns display sharp peaks at 27°,36°, 41°, 54°, and 56° corresponding to the (110), (101), (111), (211), and (220) rutile phase planes, respectively (ICDD. 996-900-9084). Diffraction peaks related to CeO_2 were not observed in the samples, suggesting that either the crystallinity of CeO_2 or the loading of CeO_2 was very low. A mean crystallite size of 17.3±0.7 nm was determined for pristine TiO_2 calculated from the Scherrer equation. No significant change in the crystallite size for the QD encrusted samples was observed through the data obtained from XRD. For the pristine CeO_2 sample, the XRD pattern obtained was identified as the cubic (fluorite group) crystal phase (ICDD 04-012-6395), with broad diffraction peaks corresponding to the nanocrystalline nature of the synthesised particles (calculated mean crystallite size is 5.17±0.04 nm).

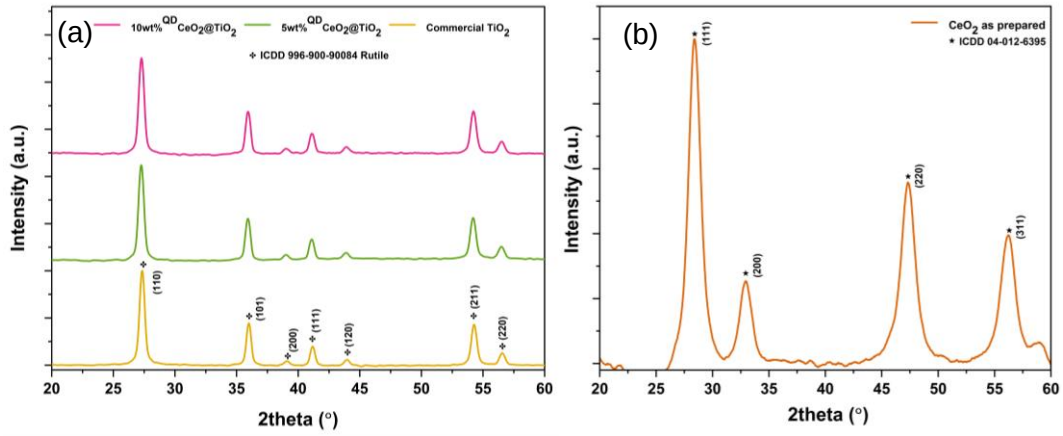

Figure 1 (a) X-ray diffraction patterns for TiO_2, $^{QD}CeO_2$@TiO_2 nanocomposites (b) X-ray diffraction patterns for pure CeO_2

Scanning Transmission Electron Microscopy (STEM) images of Pure TiO_2 (rutile) and 10%wt$^{QD}CeO_2$@TiO_2 are presented in Figure 2. The HAADF image in Figure 2(a) reveals the crystalline pure TiO_2 structure, and the calculated lattice spacing for rutile was 0.32 nm,

corresponding to the (110) plane[19]. Figure 2(b) shows the crystalline nature of CeO_2 at the surface edge, as further confirmed by the FFT inset. The inverse FFT and profile of the selected area in (b), as marked in green, were used to calculate the lattice spacing of the CeO_2 structure, which was found to be 0.27 nm and was well-aligned with the corresponding d spacing for the (200) plane of CeO_2[20]. The measured mean particle size of the CeO_2 quantum dots is 3.32±0.71 nm.

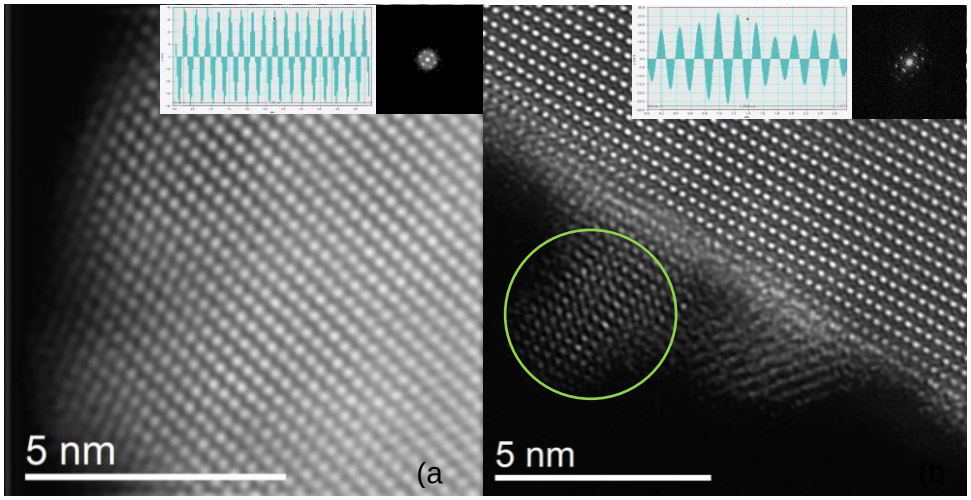

Figure 2 High-angle Annular Dark Field Scanning Transmission Electron Microscopy (HAADF STEM) image with insets of Fast Fourier Transform (FFT) pattern and Inverse FFT profiles for (a) pure TiO_2 (rutile) and (b) 10%wt$^{QD}CeO_2$@TiO_2

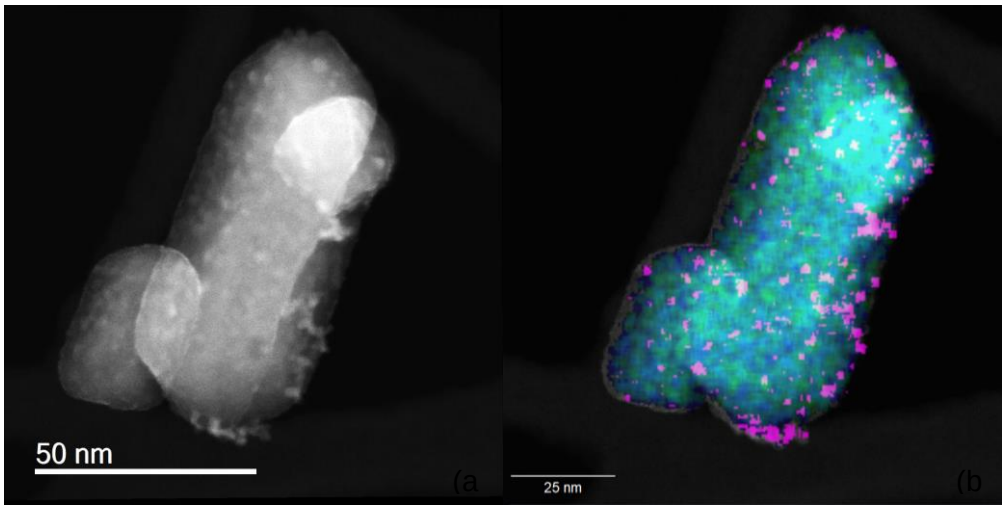

Figure 3 (a) HAADF STEM image used for EDS mapping and (b) Overlapping spectral map for 10wt% $^{QD}CeO_2$@TiO_2 sample showing the elemental distribution of Ti (blue), O (green) and Ce (Magenta)

Figure 3 presents the EDS Energy Dispersive Spectroscopy (EDS) mapping of 10wt% $^{QD}CeO_2$@TiO_2 sample. The images show CeO_2 dots attached to the TiO_2 surface without continuously coating the particle surface. The calculated weight percentage of Ce/Ti was found to be 9.73±1.28, as determined by the extracted spectra.

3.2. Optical Properties and photocatalytic activity (PCA) of nanocomposites

The effect of adding CeO_2 QDs on the UV absorption properties and optical bandgap of TiO_2 was studied using UV-vis spectroscopy as presented in Figure 4(a). TiO_2 nanoparticles are commonly used in sunscreen formulations due to their broad absorption across the UVB and short UVA regions, as shown in the figure. The composite particles have similar UV absorption bandwidths with enhanced absorption intensity. The increase in absorption intensity of the composite samples can be attributed to the scattering of incident photons by the irregular placement of CeO_2 on the TiO_2 surface, which explains the slight increase in absorption intensity across all wavelengths. Furthermore, from the calculated optical Eg values of these materials (Table 2), using Tauc plots derived from Eq. (1), it is evident that the incorporation of CeO_2 on the surface does not negatively affect the absorption and optical band gap of TiO_2.

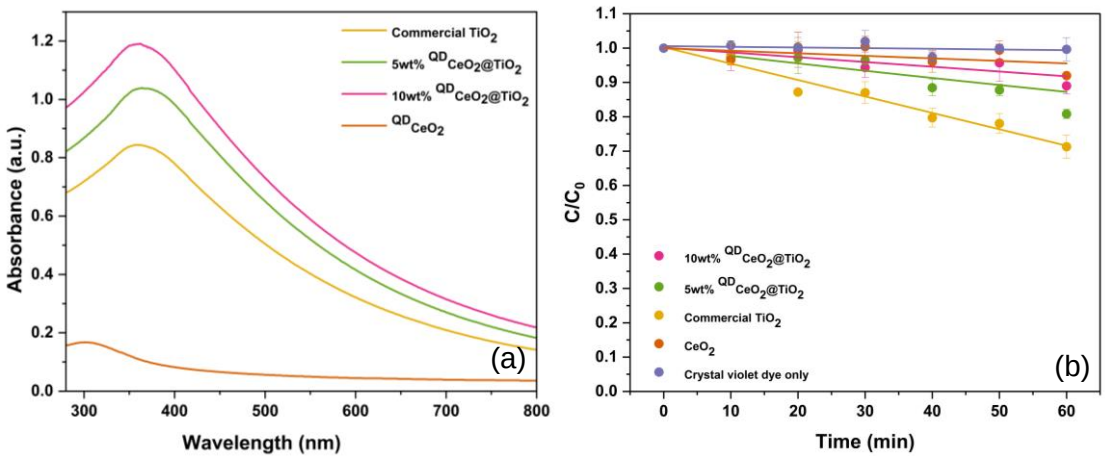

Figure 4 (a) UV–vis absorption spectra and (b) Comparison of photocatalytic degradation of crystal violet due to commercial TiO_2 and $^{QD}CeO_2@TiO_2$ composites.

The photoactivity of the synthesised material was assessed by studying the degradation of crystal violet upon exposure to UV. A comparison of the photocatalytic degradation of crystal violet due to commercial TiO_2 and $^{QD}CeO_2@TiO_2$ composites is presented in Figure 4 (b).

Table 2 Calculated optical Eg and Fluorescence peak intensities for Commercial TiO_2 (rutile) and $^{QD}CeO_2@TiO_2$ nanoparticles.

	Optical Eg (eV)	Fluorescence peak		Degradation rate constant k (10^{-3} min^{-1})
		Wavelength (nm)	Intensity (10^6 Counts.s^{-1})	
Commercial TiO_2	2.74±0.02	678.06±0.02	38.8±0.4	5.1±0.2
5wt%$^{QD}CeO_2$ @TiO_2	2.71±0.02	678.28±0.03	40.0±0.3	2.8±0.1

10wt%$^{QD}CeO_2$ @TiO_2	2.67±0.03	679.03±0.03	40.9±0.2	1.5±0.4
Pure CeO_2	3.41±0.05	NA	NA	0.8±0.1

Table 2 presents the calculated optical bandgap, fluorescence peak intensities and dye degradation constant of the TiO_2 nanoparticles and composites.The fluorescence measurements at the emission peak, around 678 nm, are slightly lower for pure TiO_2, with the peak slightly red shifting and the intensity increasing as the CeO_2 loading increases. This suggests that surface encrustation with CeO_2 promotes charge recombination via radiative pathways, potentially contributing to deactivating the excited state of TiO_2 and inhibiting photocatalysis[12], [21]. The degradation of dyes has been previously ascribed to a pseudo-first-order reaction using the Langmuir-Hinshelwood model. Commercial rutile has a degradation rate of 31%. 5%wt, and 10%wt CeO_2 encrusted TiO_2 nanocomposites reduced photocatalysis by 15% and 10%, respectively. This reduction in photocatalysis can be attributed to the change in surface properties of TiO_2 resulting from CeO_2 encrustation, which facilitates improved charge trapping. Furthermore, it has been reported that the small size of CeO_2 quantum dots is crucial for their redox activity. The coexistence of the 3+/4+ oxidation states of Ce and the presence of Ce^{3+} surface sites, along with oxygen vacancies, enables the antioxidant properties and the ability to scavenge reactive oxygen species (ROS)[17]. These factors may contribute to the lower photocatalytic activity of the nanocomposites.

3.3. In-house in vitro SPF measurements

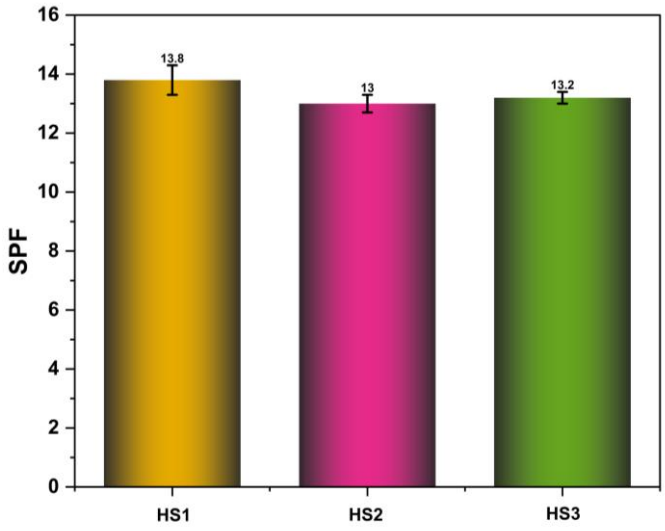

Figure 5 Non-irradiated in vitro SPF values of the homemade sunscreen formulations

The calculated in vitro SPF values of the formulations made with TiO_2 nanoparticles, 10wt%$^{QD}CeO_2$@TiO_2 and 5wt%$^{QD}CeO_2$@TiO_2 nanocomposites are 13.8±0.5, 13.0±0.3 and 13.2±0.2, respectively, as presented in Figure 5.

The homemade sunscreen formulations show comparable non-irradiated in vitro SPF values with 5 %w/W concentration of nanoparticles added to the formulation to previously reported SPF values between 5-15[22], [23], [24]. However, the formulation characteristics depend on the homogenous dispersion of the nanoparticles and the synergetic effects of the ingredients. The nanocomposites have shown excellent homogeneity in dispersion in formulation, delivering a high SPF with only 5 %w/W nanoparticles added.

4. Conclusion

Commercially used TiO_2 nanoparticles in sunscreen products have the potential to generate free radical species, such as reactive oxygen species (ROS), when exposed to UV radiation. Such free radical species have been shown to cause oxidative damage not only to human cell lines but also to other active sunscreen ingredients, resulting in a loss of protection. Thus, suppression of the photocatalytic activity of these particles while maintaining adequate UV attenuation is essential for their continued safe use in such products. Adding free radical scavenging CeO_2 QDs, obtained through a simple precipitation method, to the surface of commercial rutile nanoparticles was employed to demonstrate an alternative to conventional coatings. It was shown that an optimal CeO_2 QD loading of 10 wt% reduced the photocatalytic activity of the core TiO_2 without compromising its UV absorptive properties. Furthermore, nanocomposites used in sunscreen formulations have shown their potential in cosmetic formulations in their synergetic effects, with homogenous dispersion of the nanocomposites. Cytotoxicity and phototoxicity studies are needed to confirm the suitability for biological applications. In conclusion, these nanocomposites have the potential to pave the way for a new generation of sunscreens formulated with novel inorganic UV filters.

5. References

[1] C. Cole, T. Shyr, and H. Ou-Yang, “Metal oxide sunscreens protect skin by absorption, not by reflection or scattering,” *Photodermatology, Photoimmunology & Photomedicine*, vol. 32, no. 1, pp. 5–10, 2016, doi: 10.1111/phpp.12214.

[2] I.-M. Low, H. M. Albetran, V. M. de la Prida Pidal, and F. K. Yam, *Nanostructured Titanium Dioxide in Photocatalysis*. Milton: Jenny Stanford Publishing, 2021. doi: 10.1201/9781003148531.

[3] J.-J. Yin *et al.*, “Phototoxicity of Nano Titanium Dioxides in HaCaT Keratinocytes – Generation of Reactive Oxygen Species and Cell Damage,” *Toxicol Appl Pharmacol*, vol. 263, no. 1, pp. 81–88, Aug. 2012, doi: 10.1016/j.taap.2012.06.001.

[4] C. M. Olsen, L. F. Wilson, A. C. Green, N. Biswas, J. Loyalka, and D. C. Whiteman, “Prevention of DNA damage in human skin by topical sunscreens,” *Photodermatol Photoimmunol Photomed*, vol. 33, no. 3, pp. 135–142, May 2017, doi: 10.1111/phpp.12298.

[5] H. Ma, A. Brennan, and S. A. Diamond, “Photocatalytic reactive oxygen species production and phototoxicity of titanium dioxide nanoparticles are dependent on the solar ultraviolet radiation spectrum,” *Environ Toxicol Chem*, vol. 31, no. 9, pp. 2099–2107, Sep. 2012, doi: 10.1002/etc.1916.

[6] T. G. Smijs and S. Pavel, “Titanium dioxide and zinc oxide nanoparticles in sunscreens: focus on their safety and effectiveness,” *Nanotechnol Sci Appl*, vol. 4, pp. 95–112, Oct. 2011, doi: 10.2147/NSA.S19419.

[7] M. C. Borrás, R. Sluyter, P. J. Barker, K. Konstantinov, and S. Bakand, “Y_2O_3 decorated TiO_2 nanoparticles: Enhanced UV attenuation and suppressed photocatalytic activity with promise for cosmetic and sunscreen applications,” *Journal of Photochemistry and Photobiology B: Biology*, vol. 207, no. December 2019, p. 111883, 2020, doi: 10.1016/j.jphotobiol.2020.111883.

[8] A. Morlando, J. McNamara, Y. Rehman, V. Sencadas, P. J. Barker, and K. Konstantinov, “Hydrothermal synthesis of rutile TiO_2 nanorods and their decoration with CeO_2 nanoparticles as low-photocatalytic active ingredients in UV filtering applications,” *Journal of Materials Science*, vol. 55, no. 19, pp. 8095–8108, 2020, doi: 10.1007/s10853-020-04598-3.

[9] *Regulation (EC) No 1223/2009 of the European Parliament and of the Council of 30 November 2009 on cosmetic products (recast) (Text with EEA relevance)*, vol. 342. 2009. Accessed: Feb. 28, 2024. [Online]. Available: http://data.europa.eu/eli/reg/2009/1223/oj/eng

[10] A. M. El-Toni, S. Yin, and T. Sato, “Control of silica shell thickness and microporosity of titania-silica core-shell type nanoparticles to depress the photocatalytic activity of titania,” *J Colloid Interface Sci*, vol. 300, no. 1, pp. 123–130, Aug. 2006, doi: 10.1016/j.jcis.2006.03.073.

[11] E. Jang, K. Sridharan, Y. M. Park, and T. J. Park, “Eliminated Phototoxicity of TiO_2 Particles by an Atomic-Layer-Deposited Al_2O_3 Coating Layer for UV-Protection Applications,” *Chemistry – A European Journal*, vol. 22, no. 34, pp. 12022–12026, 2016, doi: 10.1002/chem.201600815.

[12] A. Morlando *et al.*, “Development of CeO_2 nanodot encrusted TiO_2 nanoparticles with reduced photocatalytic activity and increased biocompatibility towards a human keratinocyte cell line,” *Journal of Materials Chemistry B*, vol. 8, no. 18, pp. 4016–4028, 2020, doi: 10.1039/d0tb00629g.

[13] K. Bogusz, M. Tehei, M. Lerch, S. X. Dou, H. K. Liu, and K. Konstantinov, “TiO_2/$(BiO)_2CO_3$ nanocomposites for ultraviolet filtration with reduced photocatalytic activity,” *Journal of Materials Chemistry C*, vol. 6, no. 21, pp. 5639–5650, 2018, doi: 10.1039/c8tc01330f.

[14] Y. Bai, Z. Li, B. Cheng, M. Zhang, and K. Su, “Higher UV-shielding ability and lower photocatalytic activity of TiO_2@SiO_2/APTES and its excellent performance in enhancing the photostability of poly(p-phenylene sulfide),” *RSC Adv.*, vol. 7, no. 35, pp. 21758–21767, Apr. 2017, doi: 10.1039/C6RA28098F.

[15] “Band gap engineering of CeO_2 nanostructure using an electrochemically active biofilm for visible light applications - RSC Advances (RSC Publishing).” Accessed: Apr. 03, 2025. [Online]. Available: https://pubs.rsc.org/en/content/articlelanding/2014/ra/c4ra00861h

[16] F. Caputo *et al.*, “Cerium oxide nanoparticles, combining antioxidant and UV shielding properties, prevent UV-induced cell damage and mutagenesis,” *Nanoscale*, vol. 7, no. 38, pp. 15643–15656, Sep. 2015, doi: 10.1039/C5NR03767K.

[17] D. Cardillo, M. Weiss, M. Tehei, T. Devers, A. Rosenfeld, and K. Konstantinov, “Multifunctional Fe_2O_3/CeO_2 nanocomposites for free radical scavenging ultraviolet protection,” *RSC Advances*, vol. 6, no. 70, pp. 65397–65402, 2016, doi: 10.1039/c6ra10951a.

[18] “Cosmetics — Sun protection test method — Determination of sunscreen UVA photoprotection in vitro ISO/FDIS 24443:2011.”

[19] X. Xia *et al.*, “Control of interface between anatase TiO_2 nanoparticles and rutile TiO_2 nanorods for efficient photocatalytic H_2 generation,” *Journal of Power Sources*, vol. 376, pp. 11–17, Feb. 2018, doi: 10.1016/j.jpowsour.2017.11.067.

[20] Y. Liu, Z. Yang, X. Zhang, Y. He, J. Feng, and D. Li, “Shape/Crystal Facet of Ceria Induced Well-Dispersed and Stable Au Nanoparticles for the Selective Hydrogenation of Phenylacetylene,” *Catal Lett*, vol. 149, no. 2, pp. 361–372, Feb. 2019, doi: 10.1007/s10562-018-02648-9.

[21] S. C. Lee, N. Hasan, H. O. Lintang, M. Shamsuddin, and L. Yuliati, “Photocatalytic removal of 2,4-dichlorophenoxyacetic acid herbicide on copper oxide/titanium dioxide prepared by co-precipitation method,” *IOP Conf. Ser.: Mater. Sci. Eng.*, vol. 107, no. 1, p. 012012, Jan. 2016, doi: 10.1088/1757-899X/107/1/012012.

[22] H. Bendová *et al.*, “In vitro approaches to evaluation of Sun Protection Factor,” *Toxicology in Vitro*, vol. 21, no. 7, pp. 1268–1275, Oct. 2007, doi: 10.1016/j.tiv.2007.08.022.

[23] C.-C. Lin and W.-J. Lin, “Sun protection factor analysis of sunscreens containing titanium dioxide nanoparticles,” *Journal of Food and Drug Analysis*, vol. 19, no. 1, Jul. 2020, doi: 10.38212/2224-6614.2181.

[24] N. Tyagi *et al.*, “Comparative analysis of the relative potential of silver, zinc-oxide and titanium-dioxide nanoparticles against UVB-induced DNA damage for the prevention of skin carcinogenesis,” *Cancer Lett*, vol. 383, no. 1, pp. 53–61, Dec. 2016, doi: 10.1016/j.canlet.2016.09.026.